Asociación Argentina
de Mecánica Computacional

Mecánica Computacional Vol XXIX, págs. 5913-5927 (artículo completo)
Eduardo Dvorkin, Marcela Goldschmit, Mario Storti (Eds.)
Buenos Aires, Argentina, 15-18 Noviembre 2010

COMPUTATIONAL ANALYSIS OF BLOOD FLOW CHARACTERISTICS IN INTRACRAINAL ANEURYSMS

Juan R. Cebral[a], Fernando Mut[a], Rainald Löhner[a] and Christopher M. Putman[b]

[a]*Center for Computational Fluid Dynamics, George Mason University, Fairfax, Virginia 22030, USA jcebral@gmu.edu, http://web.cos.gmu.edu/~jcebral*

[b]*Interventional Neuroradiology, Inova Fairfax Hospital,Falls Church, Virginia 22040, USA christopher.putman@inova.com*

Keywords: Hemodynamics, Cerebral Aneurysms, Rupture Risk.

Abstract. Image-based computational fluid dynamics modeling of cerebral aneurysms has matured over the last decade. These techniques have allowed the study of patient-specific hemodynamics to better understand the mechanisms responsible for aneurysm formation, progression and rupture, and the effects of different devices and therapeutic options. The purpose of this study was to enhance and use a computational modeling chain previously developed to construct patient-specific models of cerebral aneurysms from three-dimensional (3D) medical images and pulsatile physiologic flows and use them to investigate and compare the hemodynamic characteristics in ruptured and unruptured aneurysms. Using this methodology, a database containing over 200 patient-specific models of brain aneurysms has been constructed from 3D rotational angiography images. The models have been run under different physiologic flow conditions, including pulsatile and steady flows. The resulting blood flow fields were visualized using a variety of techniques in order to qualitatively classify the aneurysms according to the following characteristics: a) flow complexity, b) flow stability, c) inflow concentration, and d) size of impingement. Secondly, a number of quantitative hemodynamic measures that attempt to capture these qualitative characteristics were defined. The aneurysms were then divided into two groups according to their previous history of subarachnoid hemorrhage, i.e. ruptured and unruptured aneurysms, and the hemodynamic characteristics of each group were analyzed and statistically compared. The results indicate that ruptured aneurysms are more likely to have concentrated inflow jets, small impaction zones, complex and unstable intra-aneurysmal flow patterns, and large maximum wall shear stress. In contrast, unruptured aneurysms tend to have diffuse inflow streams, large zones of flow impaction, simple and stable flow patterns, and lower maximum wall shear stress. The importance of these results is that these associations could be used to discriminate between mechanisms of aneurysm wall weakening based on low or high flow theories and to improve aneurysm risk evaluation which is currently only based on aneurysm geometry.

1 INTRODUCTION

Assessing the risk of rupture of intracranial aneurysms is important for clinicians because the natural rupture risk can be exceeded by the small but significant risk carried by current treatments (Kassell, Torner et al. 1990; Tomasello, D'Avella et al. 1998; Wiebers, Whisnant et al. 2003). To date, risk assessment is mainly based on aneurysm size. However, it is known that small aneurysms do rupture, and therefore a more precise risk assessment is highly desirable. Improving current aneurysm risk assessment and evaluation requires knowledge of the underlying mechanisms governing the natural evolution of cerebral aneurysms. Although these mechanisms are poorly understood, hemodynamics is thought to play a fundamental role (Stehbens 1972; Kayembe, Sasahara et al. 1984; Nixon, Gunel et al. 2009; Sforza, Putman et al. 2009). Thus, numerous investigators have used image-based computational fluid dynamics (CFD) models to extract patient-specific hemodynamics information (Jou, Quick et al. 2003; Steinman, Milner et al. 2003; Shojima, Oshima et al. 2004). However, there is no consensus on which variables or hemodynamic characteristics are the most important. This paper describes a computational framework to study and characterize both qualitatively and quantitatively the hemodynamic environment of cerebral aneurysms in order to relate it to clinical events such as growth or rupture. In particular, a number of hemodynamic quantities are proposed to describe the most salient features of these hemodynamic environments and further our understanding of the mechanisms of aneurysm progression and rupture.

2 METHODS

2.1 Patient Data

Anatomical images of cerebral aneurysms and the connected arteries are obtained using 3D rotational angiography (3DRA) during conventional transfemoral catheterization of the cerebral blood vessels. Rotational acquisitions are obtained during a six seconds contrast injection for a total of 24 cc of contrast agent on a Philips Integris biplane unit (Philips Medical Systems, Best, The Netherlands). The projection images are reconstructed into 3D voxel data using standard proprietary software (Philips XtraVision). The patients' medical and radiological records are reviewed and evaluated for evidence of aneurysmal intracranial hemorrhage. In patients with multiple aneurysms, the clinical and radiological information are considered and a judgment of the most likely source of hemorrhage is made. The other co-incident aneurysms are classified as unruptured. Cases with evidence of vasospasm, or incomplete or inconclusive clinical information as well as dissecting aneurysms are excluded from the study.

2.2 Anatomical Modeling and Meshing

Patient-specific vascular models are constructed from the 3DRA images using seeded region growing segmentation to recover the arterial network topology followed by iso-surface deformable models to recover the vascular geometry (Yim, Boudewijn et al. 2003; Cebral, Castro et al. 2005). The models are then smoothed using a non-shrinking algorithm (Taubin 1995) and arterial branches are truncated perpendicularly to their axes. During the vascular model construction process, the entire proximal portion of the parent artery visible in the 3D image is included in the model to ensure proper representation of secondary or swirling flows at the aneurysm location (Castro, Putman et al. 2006). The geometrical models are then used to generate volumetric computational grids composed of tetrahedral elements using an advancing front method (Löhner 2001; Cebral, Castro et al. 2005). These meshes are generated with a minimum uniform resolution of 0.01 cm to 0.02 cm. The mesh resolution is locally increased using source functions along arterial branches in order to ensure a minimum of 10 to 20 grid points in all vessel diameters. Typical meshes contain between 1 million and 5 million elements.

2.3 Geographic Model Subdivision

For subsequent analysis the computational mesh is partitioned into different geographic regions. This process consists of the following steps: a) interactive delineation of the aneurysm neck, b) triangulation of the aneurysm orifice, c) partition of the computational domain into aneurysm and vessel regions, d) further subdivision of aneurysm and vessel regions into sub-regions. During the interactive neck delineation, the user clicks on grid points along the aneurysm neck that are connected along the shortest geodesic path. Then, the aneurysm orifice defined by this neck contour is triangulated. This neck surface is then used to split the surface and volume grids into two regions corresponding to the aneurysm and the connected arteries. This is done by identifying all edges of the surface and volume grids that are cut by the triangles of the neck surface and using a region growing algorithm to label all grid points on each side of the neck surface. Subsequently, signed geodesic distance to the neck is computed on the surface and volume grids. These maps are then used to further subdivide the vessel and aneurysm regions into the following sub-regions: 1) near vessel – negative distance to the neck less than 1 cm, 2) far vessel – negative distance to the neck larger than 1 cm, 3) aneurysm neck – positive distance to the neck less than 10% of maximum positive distance, 4) aneurysm body – positive distance to the neck less than 60% of the maximum positive distance, and 5) aneurysm dome - positive distance to the neck larger than 60% of the maximum positive distance. The procedure is illustrated in Figure 1.

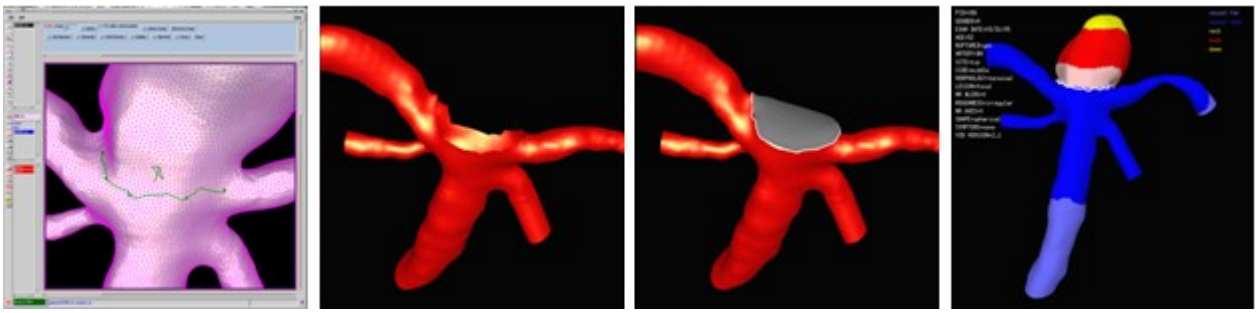

Figure 1: Geographic subdivision of vascular model. Left to right: neck delineation, aneurysm removal, neck orifice triangulation, geographic regions labeling.

2.4 Blood Flow Modeling

Blood flows are mathematically modeled using the unsteady 3D Navier-Stokes equations for an incompressible Newtonian fluid with density ρ=1.0 g/cm^3 and viscosity μ=0.04 Poise. The governing equations are advanced in time using a fully implicit scheme that recasts the original equations as a steady-state problem in pseudo-time (ϑ) at each time-step (n):

$$u^{\xi}_{,\vartheta} + u^{\xi} \cdot \nabla u^{\xi} + \nabla p^{\xi} = \nabla \eta \, \nabla u^{\xi} - \frac{u^{\xi} - u^{n}}{\xi \, \Delta t} \tag{1}$$

$$\nabla \cdot u^{\theta} = 0 \tag{2}$$

where u is the velocity, p the pressure, η the kinematic viscosity, u^n denotes the velocity at the previous timestep and $u^{\xi}=(1-\xi)\, u^{n} + \xi \, u^{n+1}$. The parameter ξ selects the numerical scheme: first order implicit Euler scheme ($\xi=1$), first order explicit Euler scheme ($\xi=0$) and second order Crank-Nicholson scheme ($\xi=1/2$). These equations are solved using a pressure-projection method where the spatial discretization is carried out using an edge-based upwind finite element method (Löhner 2001). The discretized momentum equation is solved using a Generalized Minimal Residuals (GMRES) method and the discretized pressure Poisson equation is solved using a deflated preconditioned conjugate gradients method (Mut, Aubry et al. 2009). This last method has been shown to significantly reduce the computation time, especially for elongated or tubular domains.

2.5 Physiologic Boundary Conditions

Typically, patient-specific blood flow data is not collected as part of the routine clinical examinations, and thus this information is not commonly available. Therefore, typical flow waveforms obtained from *in vivo* measurements of blood flows in normal subjects using phase-contrast magnetic resonance are used to prescribe boundary conditions (Cebral, Castro et al. 2003; Ford, Alperin et al. 2005; Cebral, Castro et al. 2008). The waveforms measured in the cerebral arteries of normal volunteers are scaled with the area of the inlet boundary in order to achieve a mean wall shear stress of 15 dyne/cm^2 at the inlet (Cebral, Castro et al. 2008). Fully developed velocity

profiles are specified at the model inlet boundary using the Womersley solution (Taylor, Hughes et al. 1998). Traction-free boundary conditions are prescribed at the model outlets. Since patient-specific flows are not known, in order to assess the variability of the hemodynamic quantities each model is run under two pulsatile flow waveforms corresponding heart rates of 60 bpm and 100 bpm (Jiang and Strother 2009), and three steady flow conditions corresponding to an inlet wall shear stress of 10 (low), 15 (medium) and 20 dyne/cm^2 (high), respectively.

2.6 Flow Post-Processing

The computed flow field is post-processed to define a number of derived quantities. These derived fields can be subdivided into: a) volumetric fields, b) surface fields, and c) fields defined at the aneurysm orifice surface, and are defined as follows.

Volumetric fields:
Derived fields defined over the domain volume include: kinetic energy (k), strain rate ($\dot{\gamma}$), viscous dissipation (Φ), and vorticity (ω), defined as:

$$k = \frac{1}{2}\rho\, u^2 \tag{3}$$

$$\dot{\gamma} = 2\sqrt{e_{ij}\, e_{ij}} \tag{4}$$

$$\Phi = \frac{1}{2}\eta\, \dot{\gamma}^2 \tag{5}$$

$$\omega = \nabla \times u \tag{6}$$

where the strain rate tensor (e_{ij}) is given by:

$$e_{ij} = \frac{1}{2}\left(\frac{\partial u_i}{\partial x_j} + \frac{\partial u_j}{\partial x_i}\right) \tag{7}$$

These fields are numerically computed from the velocity field using a Galerkin finite element approximation in the volumetric domain Ω.

Surface fields:
Surface fields derived over the domain surface include the wall shear stress (τ), which is calculated as the derivative of the tangential velocity (u_t) in the normal direction (n) at the vessel surface:

$$\tau = \frac{\partial u_t}{\partial n} \tag{8}$$

This field is computed from the velocity field using a parabolic recovery of boundary gradients method (Löhner, Appanaboyina et al. 2007) which is a second order method equivalent to placing three grid points in the boundary layer.

Orifice fields:
Finally, the velocity field is interpolated to the orifice surface Γ_o. This is done by first identifying all the edges of the volume grid that are cut by triangles of the surface

defining the neck surface. The algorithm uses a bin data structure to store all the edges of the volume grid. Then it loops over all the neck surface triangles and identifies from the bin structure the edges crossing the bounding box of each triangle. These edges are tested to check whether they cut the triangle plane and if so, if the intersection point lies inside the triangle, in which case the edge is marked as cut. Once the cut edges have been found, linear interpolation is used to compute the field values at the intersection points. A triangular connectivity is then generated connecting the intersection points into an interpolated neck surface mesh. Using this connectivity the surface normal at each point on the orifice surface is computed and used to find the velocity components along the normal (u_n) and tangential (u_t) directions.

2.7 Hemodynamics Characterization

The aneurismal hemodynamic environment is qualitatively characterized by visual inspection of a set of blood flow visualizations according to the following properties (Cebral, Mut et al. 2010): 1) Flow complexity: simple flow patterns consisting on a single recirculation zone or vortex structure within the aneurysm, or complex flow patterns exhibiting flow divisions or separations within the aneurysm sac and containing more than one recirculation zone or vortex structure; 2) Flow stability: stable flow patterns that persist (do not move or change) during the cardiac cycle, or unstable flow patterns where the flow divisions and/or vortex structures move or are created or destroyed during the cardiac cycle; 3) Inflow concentration: concentrated inflow streams or jets that penetrate relatively deep into the aneurysm sac and are thin or narrow in the main flow direction, or diffuse inflow streams that are thick compared to the aneurysm neck and flow jets that disperse quickly once they penetrate into the aneurysm sac; and 4) Flow impingement: The flow impingement zone is the region of the aneurysm where the inflow stream is seen to impact the aneurysm wall and change its direction and/or disperse. This region is classified as small (large) if its area is small (large) compared to the area of the aneurysm (less than 50% or more than 50%). Examples are presented in Figure 2.

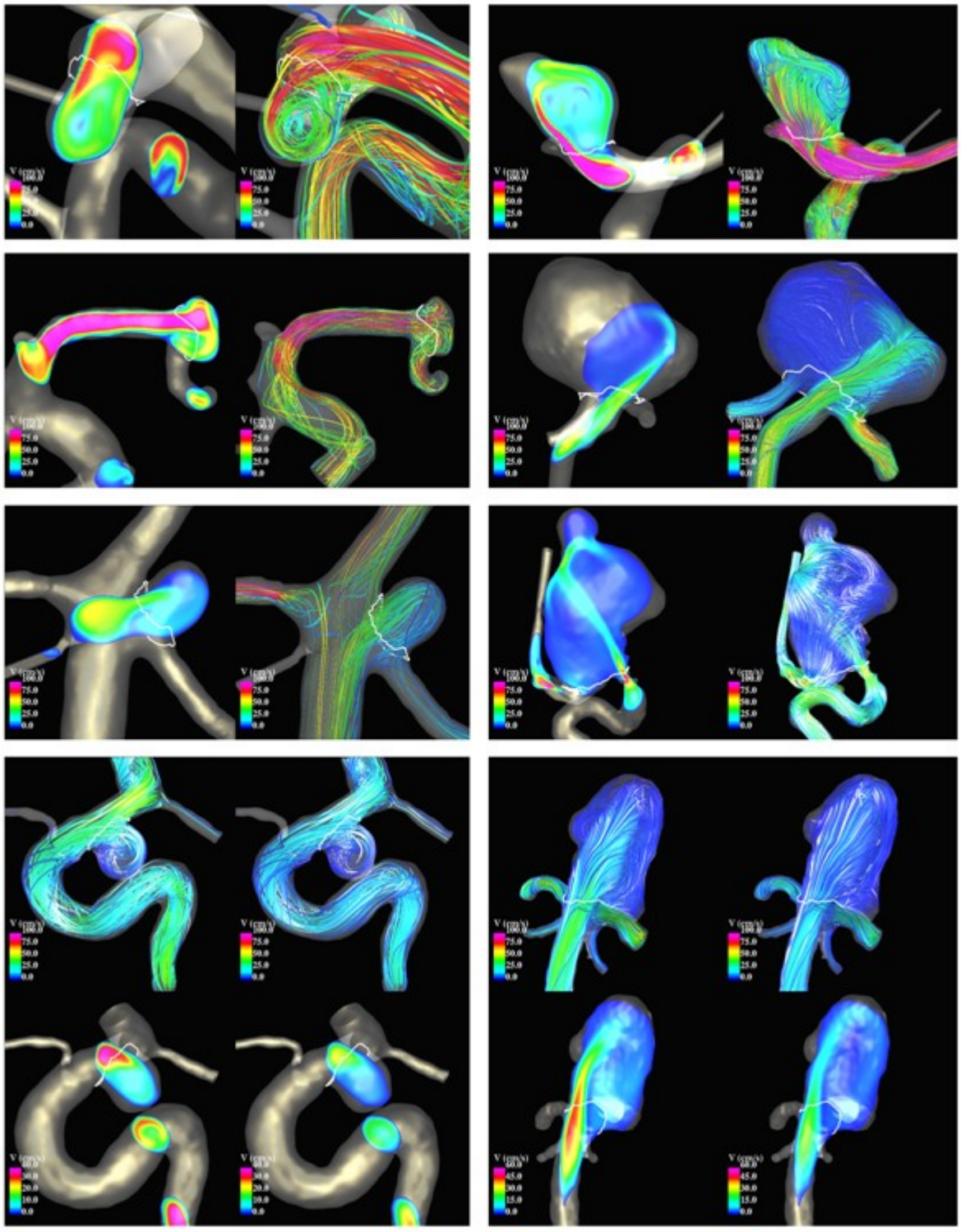

Figure 2: Examples of aneurysm flow characteristics. Top to bottom and left to right: simple and complex flows, large and small impingement regions, diffuse and concentrated inflows, and stable and unstable flow patterns.

2.8 Data Reduction

Using the geographic subdivision described earlier, the following quantities are

defined using hemodynamic variables defined over the volume, surface or orifice regions:

Kinetic Energy Ratio (KER): measures the total kinetic energy in the aneurysm relative to that of the parent artery:

$$KER = \frac{k_a}{k_v} = \frac{\int_{\Omega_a} \frac{1}{2} \rho u^2 d\Omega}{\int_{\Omega_v} \frac{1}{2} \rho u^2 d\Omega} \tag{9}$$

where k_a and k_v represent the total kinetic energy computed over the aneurysm (Ω_a) and near vessel regions (Ω_v), respectively.

Viscous Dissipation Ratio (VDR): measures the amount of viscous dissipation of mechanical energy in the aneurysm relative to that in the parent artery:

$$VDR = \frac{\Phi_a}{\Phi_v} = \frac{\int_{\Omega_a} \frac{1}{2} \eta \dot{\gamma}^2 d\Omega}{\int_{\Omega_v} \frac{1}{2} \eta \dot{\gamma}^2 d\Omega} \tag{10}$$

where Φ_a and Φ_v represent the total mechanical dissipation in the aneurysm and near vessel regions, respectively.

Maximal wall shear stress (MWSS): measures the maximum wall shear stress value over the aneurysm region:

$$MWSS = \max_{\Gamma_a} (\tau) \tag{11}$$

Denoting τ_v and σ_v the mean and standard deviation of the wall shear stress magnitude computed over the near vessel region, aneurysm regions of high (Γ_h) and low (Γ_l) wall shear stress are defined as regions where the WSS is higher or lower than the mean WSS in the parent artery by one standard deviation:

$$\begin{aligned} \Gamma_h &= \{x \in \Gamma_a \,/\, \tau(x) > \tau_v + \sigma_v\} \\ \Gamma_l &= \{x \in \Gamma_a \,/\, \tau(x) < \tau_v - \sigma_v\} \end{aligned} \tag{12}$$

The areas of these two regions are denoted by A_h and A_l, respectively. In addition to MWSS, the following surface variables are defined:

Low Shear Area (LSA): measures the percent of the aneurysm area that is subject to a "low" WSS, i.e. one standard deviation below the mean WSS in the parent artery:

$$LSA = A_l / A_a \tag{13}$$

where A_a is the area of the aneurysm sac. This variable is 0 if there is no region with WSS below one standard deviation of the mean WSS in the parent artery, and will tend to 1 if the entire aneurysm is subject to "low" WSS.

Shear Concentration Index (SCI): measures the degree of concentration of the WSS distribution:

$$SCI = \frac{F_h \,/\, F_a}{A_h \,/\, A_a} \tag{14}$$

where F_h and F_a represent the total viscous shear force computed over the region of WSS (Γ_h) and the entire aneurysm (Γ_a), respectively:

$$F_h = \int_{\Gamma_h} |\tau| \, d\Gamma \,, \quad F_a = \int_{\Gamma_a} |\tau| \, d\Gamma \tag{15}$$

This index becomes 0 if no part of the aneurysm is under "high" WSS (higher than one standard deviation above the mean WSS in the parent artery) and becomes large when the WSS distribution has a peak with high WSS concentrated on a small region of the aneurysm.

Low Shear Index (LSI): measures the relative amount of the total shear force that is applied in regions of "low" WSS:

$$LSI = \frac{F_l \, A_l}{F_a \, A_a} \tag{16}$$

where F_l is the total viscous shear force applied in the region of "low" WSS:

$$F_l = \int_{\Gamma_l} |\tau| \, d\Gamma \tag{17}$$

The *LSI* varies from 0 when no frictional shear force is applied in regions of low WSS to 1 when the total frictional shear force is applied in regions of low WSS.

Defining Γ_i the inflow region of the aneurism orifice, i.e. with positive normal velocity:

$$\Gamma_i = \{x \in \Gamma_o \,/\, u_n > 0 \;\} \tag{18}$$

the areas of the inflow and entire aneurysm orifice are denoted as A_i and A_o, respectively.

Inflow Concentration Index (ICI): measures the degree of concentration of the blood stream flowing from the parent artery into the aneurysm:

$$ICI = \frac{Q_i \,/\, Q_v}{A_i \,/\, A_o} \tag{19}$$

where Q_v is the flow rate in the parent artery and Q_i is the flow rate entering the aneurysm:

$$Q_i = \int_{\Gamma_i} u_n \, d\Gamma \tag{20}$$

This index takes a value of 0 if no flow enters the aneurysm and grows larger as the flow rate increases and is concentrated over a small region of the aneurysm orifice.

3 RESULTS

A total of 210 cerebral aneurysms have been modeled and analyzed as described before. For each aneurysm, the values of all the variables defined above were computed at each instant of time during the cardiac cycle and their minimum, maximum and average values over the cardiac cycle were calculated. Then, different aneurysm groups were defined including ruptured and unruptured aneurysms,

aneurysms with complex or simple flows, aneurysms with stable or unstable flows, aneurysms with concentrated or diffuse inflows, and aneurysms with small or large flow impingement regions. The average values of these variables over the different aneurysm groups were then computed and statistically compared using Student's t-test. The differences in the mean values were considered statistically significant if the two-tailed p-values were less than 0.05 (95% confidence).

The results are summarized in Table 1. This table lists the number of ruptured and unruptured aneurysms in each qualitative flow category, the mean values of the hemodynamic variables over the ruptured and unruptured groups as well as the p-values of the corresponding t-tests.

	Variable	Ruptured	Unruptured	P-value
Hemodynamic characteristics	simple flow	14	62	<0.0001
	complex flow	69	65	
	stable flow	20	59	0.0018
	unstable flow	63	68	
	diffuse inflow	28	85	<0.0001
	concentrated inflow	55	42	
	large impingement	20	62	0.0006
	small impingement	63	65	
Hemodynamic measures	MWSS	384 dyn/cm^2	277 dyn/cm^2	0.0034
	ICI	1.012	0.66	0.0035
	SCI	9.97	6.47	0.0154
	VDR	0.36	0.951	0.0123
	KER	0.232	0.176	0.2226
	LSA	60%	56%	0.3716
	LSI	0.26	0.25	0.6630
Geometry	size	9.38 mm	6.59 mm	<0.0001
	AR	1.42	0.966	<0.0001

Table 1: Hemodynamic characteristics and quantitative measures of ruptured and unruptured aneurysms.

The ratios of the number of ruptured to unruptured aneurysms in each flow category are presented in Figure 3. The stars over the bars indicate statistically significant differences.

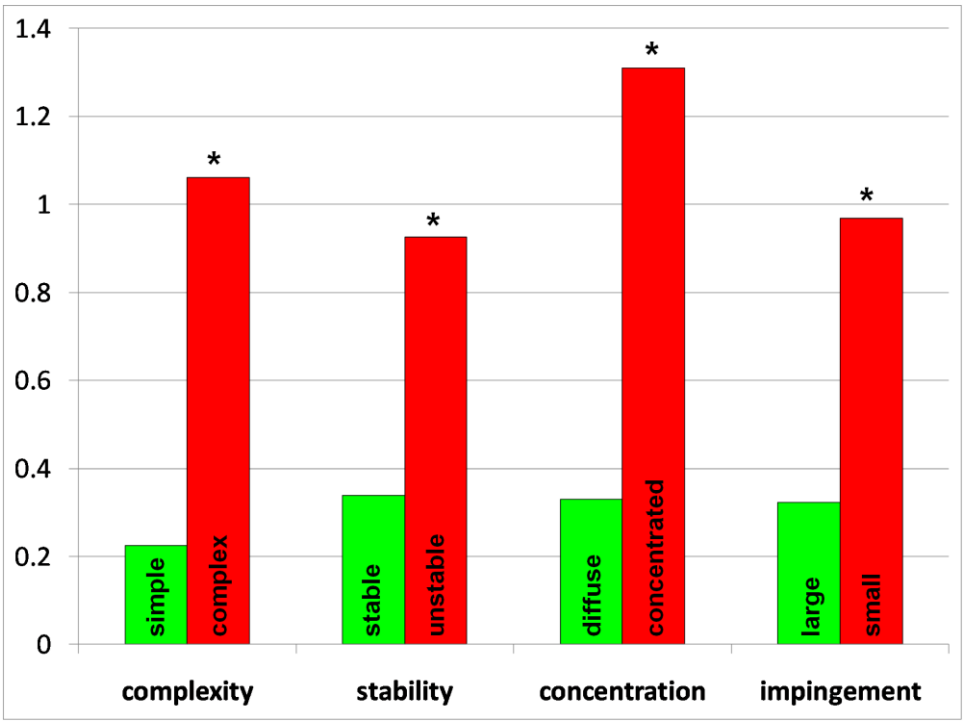

Figure 3: Qualitative hemodynamic characteristics and aneurysm rupture.

Similarly, the ratios of the mean values of geometric and hemodynamic variables of ruptured to unruptured aneurysm groups are shown in Figure 4. Bars above (below) one mean values larger (smaller) for the ruptured group. The error bars included in this figure represent the variability of these ratios of hemodynamic quantities with the different physiologic flow conditions considered. Again, the starts indicate statistically significant differences (to 95% levels) in the values of quantities over the ruptured and unruptured groups. The plus sign indicates a marginal significance to a 90% level.

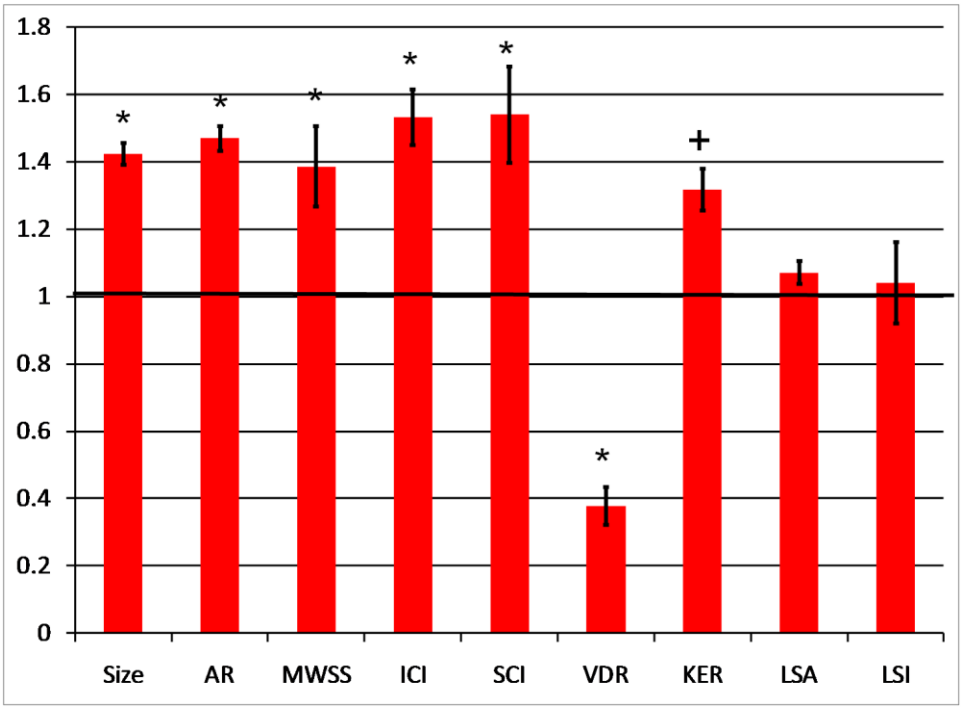

Figure 4: Quantitative measures and aneurysm rupture.

These results indicate that ruptured aneurysms are more likely to have complex flows, unstable flow patterns, concentrated inflows and small impingement regions than unruptured aneurysms. These qualitative characteristics are consistent with values of hemodynamic variables that indicate that ruptured aneurysms tend to have larger inflow concentration indices, larger shear concentration indices, larger maximal wall shear stress, marginally larger kinetic energy ratios, and smaller viscous dissipation ratios that unruptured aneurysms. Additionally, ruptured aneurysms are on average bigger and of larger aspect ratios than unruptured aneurysms. In contrast, ruptured and unruptured aneurysms did not have significant differences in their areas under low wall shear stress or in their low shear indices.

Finally, the ratios of hemodynamic quantities averaged over the different qualitative hemodynamic categories defined earlier are presented in Figure 5. As in the previous figures starts (and plus signs) indicate statistically significant differences between the values of these quantities over the different aneurysm groups. These results indicate that complex flows tend to be associated with higher maximal WSS, more concentrated inflows, more concentrated shear stress distributions, larger areas of low WSS and lower viscous dissipation ratios than simple flows. Unstable flows are associated to larger inflow and shear stress concentrations, larger areas of low WSS and larger low shear indices, and lower viscous dissipation ratios than stable flows. Aneurysms classified as having concentrated inflows tend to have larger maximal WSS, inflow and shear concentrations, areas under low WSS and low shear indices, and lower viscous dissipation ratios than those classified as having diffuse inflows. Similarly, aneurysms with small impingement regions were found to have larger shear

concentration indices, areas of low WSS and low shear factors, and lower viscous dissipation and kinetic energy ratios than aneurysms with large impingement regions.

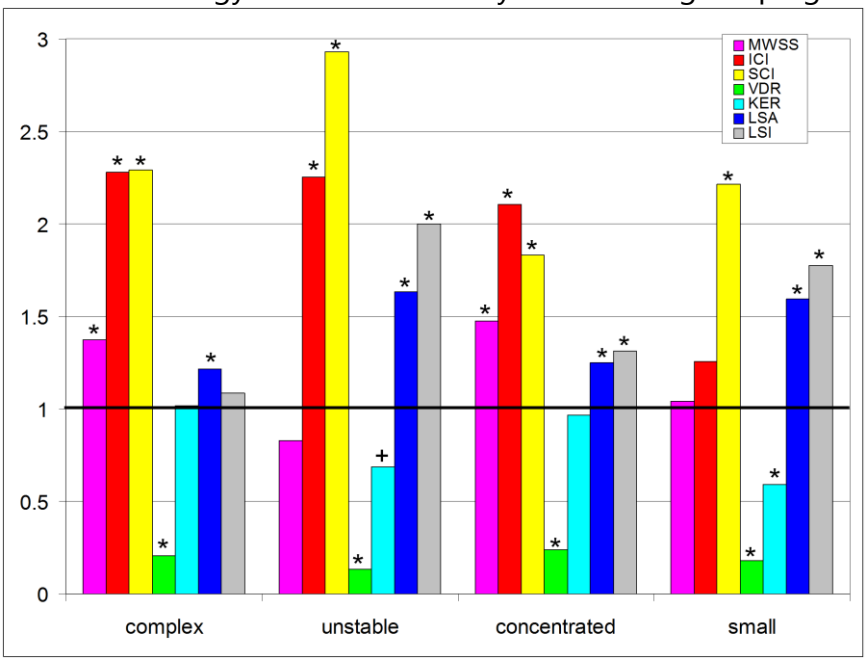

Figure 5: Relationship between hemodynamic characteristics and quantitative measures.

4 CONCLUSIONS

A computational framework for the analysis of hemodynamics of cerebral aneurysms has been described. A number of qualitative characteristics and quantitative measures have been defined and obtained over a patient population with a total of 210 cerebral aneurysms. This analysis indicates that ruptured aneurysms tend to have concentrated inflows, concentrated wall shear stress distributions, higher maximal wall shear stress and smaller viscous dissipation ratios than unruptured aneurysms. Additionally, ruptured aneurysms tended to be larger in size and to have larger aspect ratios than unruptured aneurysms, as expected. All these associations reached a strong statistical significance. In addition, these statistical associations were found to be largely unaffected by the choice of physiologic flow conditions even if steady flows are used. This confirms the notion that hemodynamic information derived from image-based CFD models can be used to assess aneurysm rupture risk, to test hypotheses about the mechanisms responsible for aneurysm formation, progression and rupture, and to answer specific clinical questions.

ACKNOWLEDGEMENTS

We thank Philips Healthcare and the NIH (grant # R01NS059063) for financial support.

REFERENCES

Castro, M. A., C. M. Putman, et al. Computational fluid dynamics modeling of

intracranial aneurysms: effects of parent artery segmentation on intra-aneurysmal hemodynamcis. *AJNR American Journal of Neuroradiology*, 27: 1703-1709, 2006.

Cebral, J. R., M. A. Castro, et al. Efficient pipeline for image-based patient-specific analysis of cerebral aneurysm hemodynamics: Technique and sensitivity. *IEEE Transactions in Medical Imaging*, 24(1): 457-467, 2005.

Cebral, J. R., M. A. Castro, et al. Flow-area relationship in internal carotid and vertebral arteries. *Physiol Meas*, 29: 585-594, 2008.

Cebral, J. R., M. A. Castro, et al. Blood flow models of the circle of Willis from magnetic resonance data. *Journal of Engineering Mathematics*, 47(3-4): 369-386, 2003.

Cebral, J. R., F. Mut, et al. Association of hemodynamic characteristics and cerebral aneurysm rupture. *AJNR American Journal of Neuroradiology*, in press, 2010.

Ford, M. D., N. Alperin, et al. Characterization of volumetric flow rate waveforms in the normal internal carotid and vertebral arteries. *Physiol Meas*, 26: 477-488, 2005.

Jiang, J. and C. M. Strother. Computational fluid dynamics simulations of intracranial aneurysms at varying heart rates: a "patient-specific" study. *J Biomech Engr*, 131(9): 091-001, 2009.

Jou, L. D., C. M. Quick, et al. Computational approach to quantifying hemodynamic forces in giant cerebral aneurysms. *AJNR American Journal of Neuroradiology*, 24(9): 1804-1810, 2003.

Kassell, N. F., J. C. Torner, et al. The International Cooperative Study on the Timing of Aneurysm Surgery. Part 1: Overall management results. *Journal of Neurosurgery*, 73(1): 18-36, 1990.

Kayembe, K. N. T., M. Sasahara, et al. Cerebral aneurysms and variations of the circle of Willis. *Stroke*, 15: 846-850, 1984.

Löhner, R. *Applied CFD techniques*, John Wiley & Sons, 2001.

Löhner, R., S. Appanaboyina, et al. Parabolic Recovery of Boundary Gradients. *Comm Num Meth Eng*, 24: 1611-1615, 2007.

Mut, F., R. Aubry, et al. Fast numerical solutions in patient-specific simulations of arterial models. *Comm Num Meth Eng*, DOI 10.1002/cnm.1235, 2009.

Nixon, A. M., M. Gunel, et al. The critical role of hemodynamics in the development of cerebral vascular disease. *J Neurosurg*, (PMID: 19943737) - in press, 2009.

Sforza, D., C. M. Putman, et al. Hemodynamics of Cerebral Aneurysms. *Ann Rev Fluid Mechanics*, 41: 91-107, 2009.

Shojima, M., M. Oshima, et al. Magnitude and role of wall shear stress on cerebral aneurysm: computational fluid dynamic study of 20 middle cerebral artery aneurysms. *Stroke*, 35(11): 2500-2505, 2004.

Stehbens, W. E. Intracranial aneurysms. *Pathology of the Cerebral Blood Vessels*. St. Louis, Misoury, CV Mosby**:** 351-470, 1972.

Steinman, D. A., J. S. Milner, et al. Image-based computational simulation of flow dynamics in a giant intracranial aneurysm. *AJNR American Journal of Neuroradiology*, 24(4): 559-566, 2003.

Taubin, G. A signal processing approach to fair surface design. *Proc. 22nd Annual*

Conference on Computer Graphics and Interactive Techniques (SIGGRAPH 1995), Los Angeles, CA, 1995.

Taylor, C. A., T. J. R. Hughes, et al. Finite element modeling of blood flow in arteries. *Computer Methods in Applied Mechanics and Engineering*, 158: 155-196, 1998.

Tomasello, F., D. D'Avella, et al. Asymptomatic aneurysms. Literature meta-analysis and indications for treatment. *Journal of Neurosurgical Science*, 42(1): 47-51, 1998.

Wiebers, D. O., J. P. Whisnant, et al. International Study of Unruptured Intracranial Aneurysms Investigators. Unruptured intracranial aneurysms: natural history, clinical outcome, and risks of surgical and endovascular treatment. *Lancet*, 362(9378): 103-110, 2003.

Yim, P. J., G. Boudewijn, et al. Isosurfaces as deformable models for magnetic resonance angiography. *IEEE Trans on Medical Imaging*, 22(7): 875-881, 2003.